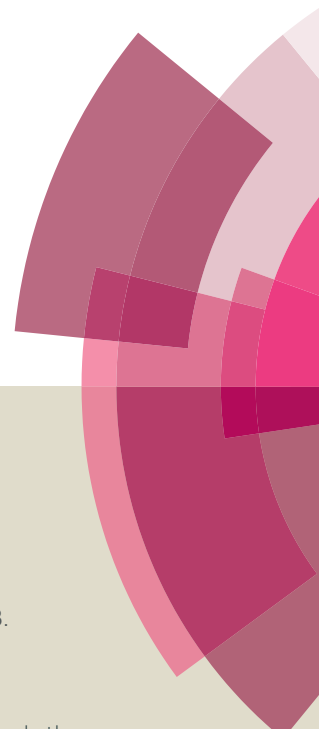


# Catalysis Science & Technology

Accepted Manuscript



This article can be cited before page numbers have been issued, to do this please use: A. K. Rathi, M. B. Gawande, V. Ranc, J. Pechousek, M. Petr, K. Cepe, R. S. Varma and R. Zboril, *Catal. Sci. Technol.*, 2015, DOI: 10.1039/C5CY00956A.



This is an *Accepted Manuscript*, which has been through the Royal Society of Chemistry peer review process and has been accepted for publication.

*Accepted Manuscripts* are published online shortly after acceptance, before technical editing, formatting and proof reading. Using this free service, authors can make their results available to the community, in citable form, before we publish the edited article. We will replace this *Accepted Manuscript* with the edited and formatted *Advance Article* as soon as it is available.

You can find more information about *Accepted Manuscripts* in the [Information for Authors](#).

Please note that technical editing may introduce minor changes to the text and/or graphics, which may alter content. The journal's standard [Terms & Conditions](#) and the [Ethical guidelines](#) still apply. In no event shall the Royal Society of Chemistry be held responsible for any errors or omissions in this *Accepted Manuscript* or any consequences arising from the use of any information it contains.



## Catalysis Science and Technology

## ARTICLE

## Continuous flow hydrogenation of nitroarenes, azides and alkenes using maghemite-Pd nanocomposites†

Received 00th January 2015,  
Accepted 00th January 2015

DOI: 10.1039/x0xx00000x

www.rsc.org/

Anuj K. Rathi,<sup>a</sup> Manoj B. Gawande,<sup>a\*</sup> Vaclav Ranc,<sup>a</sup> Jiri Pechousek,<sup>a</sup> Martin Petr,<sup>a</sup> Klara Cepe,<sup>a</sup> Rajender S. Varma<sup>b</sup> and Radek Zboril<sup>a\*</sup>

Maghemite-supported ultra-fine Pd (1-3 nm) nanoparticles, prepared by a simple co-precipitation method, find application in the catalytic continuous flow hydrogenation of nitroarenes, azides, and alkenes wherein they play an important role in reduction of various functional groups on the surface of maghemite with catalyst loading (~6 wt%). The salient features of the protocol include expeditious formation of reduced products in high yields at near ambient conditions with recycling of the catalyst (up to 12 cycles) without any loss in selectivity and yield.

## Introduction

Aromatic amines and its derivatives are employed in various important organic intermediates for the production of dyes, polymers in pharmaceutical industry and are frequently obtained via the reduction of nitro compounds.<sup>1</sup> The reduction of C=C double and triple bonds, and other functional groups utilize various catalysts that include noble metals (Pt, Pd, Ru, and Rh)<sup>2</sup> as well as non-noble metals (Co, Ni and Cu)<sup>3</sup> catalysts under a variety of reaction conditions; each reported catalytic protocol has its own advantages and disadvantages. Keeping in mind the importance of amines and alkanes in commodity chemicals and pharmaceuticals, catalytic hydrogenation reactions have been investigated under a variety of energy input systems namely microwave irradiation, ultrasonication, and ball milling or using benign solvent-free and water-mediated protocols.<sup>4</sup> However, despite these significant advancements, catalytic hydrogenation reactions can still benefit from sustainable improvements.

Continuous flow reactions are receiving tremendous interest for applications in the development of selective processes because of their intrinsic advantages, when compared to conventional batch reactions; the ease of isolation or purification, reduction in waste emissions, safety, automation, and space-time-yield efficiency being

prominent.<sup>5</sup>

The chemoselective and partial catalytic hydrogenation of functionalized hydrocarbons with multiple C=C and C≡C bonds is a very desirable trait and prerequisite in the pharmaceutical and petrochemical industries.<sup>6</sup> In general, the catalytic hydrogenation reaction (reduction of nitro compounds, C=C and C≡C bonds) often deploy various types of heterogeneous and noble metal supported catalysts under continuous flow conditions.<sup>7</sup> However, in most cases, catalysts cannot be reused and recycled or plagued by leaching of metals due to high pressure and related reaction parameters in flow reactor.<sup>8</sup> Consequently, it is prudent to design stable, cost-effective, and reusable catalytic system for hydrogenation reactions.

In recent years, there is a remarkable rise in the exploitation of magnetic nanocomposites because of their preparation from inexpensive precursors, inert and stable nature and most importantly, their reusable and recyclable feature for several runs without impairment of catalytic activity and selectivity.<sup>9</sup> It is not surprising, therefore, that there is enormous demand for magnetically recyclable nanocatalysts in continuous flow processes.<sup>5c</sup> Herein, we describe hydrogenation reactions for the reduction of nitro-, azide-, and alkene functionalities under continuous flow on recyclable maghemite decorated with Pd nanoparticles (Fig. 1).

## Experimental

## Materials and reagents

All commercial reagents were used as received unless otherwise mentioned. For analytical and preparative thin-layer chromatography (TLC), Merck, 0.2 mm and 0.5 mm Kieselgel GF 254 pre-coated were used, respectively. The spots were visualized with iodine, and UV light. The reactions were performed on Thales Nano H-Cube continuous flow hydrogen reactors, utilising water electrolysis to generate hydrogen. The conversion and selectivity of the individual hydrogenation

<sup>a</sup>Regional Centre of Advanced Technologies and Materials, Department of Physical Chemistry, Faculty of Science, Palacky University, Šlechtitelů 11, 783 71, Olomouc, Czech Republic. E-mail addresses: manoj.gawande@upol.cz (Manoj Gawande) and radek.zboril@upol.cz (Radek Zboril).

<sup>b</sup>Sustainable Technology Division, National Risk Management Research Laboratory, US Environmental Protection Agency, 26 West Martin Luther King Drive, MS 443, Cincinnati, Ohio, 45268, USA.

† Electronic Supplementary Information (ESI) available: Materials and reagents used, description of characterization techniques employed, TEM images of fresh catalyst and reused catalyst, values of the Mössbauer hyperfine parameters, derived from the spectra fitting, and conversion values after reusability. See DOI: 10.1039/x0xx00000x

## ARTICLE

reactions were analyzed by GC employing chromatograph Agilent 6820 (Agilent, United States) equipped with flame ionisation detector (FID) and chromatographic column DB5 (30x0.250x0.25). Following experimental parameters were applied: initial temperature 100 °C, increased to 250°C with a rate of 10 °C/min. Yield determined using internal standard.

**Synthesis of maghemite ( $\gamma$ -Fe<sub>2</sub>O<sub>3</sub>) nanoparticles**

Magnetically separable maghemite was prepared by the chemical co-precipitation and dehydration method. Typically, FeSO<sub>4</sub>·7H<sub>2</sub>O (6.06 g, 21.79 mmol) and FeCl<sub>3</sub>·6H<sub>2</sub>O (11.75 g, 45.08 mmol) were dissolved in 100 mL of deionised water (previously degassed with nitrogen) under N<sub>2</sub> atmosphere. The resulting mixture was stirred for 30 minutes and heated at 60 °C under vigorous stirring. When the temperature reached to 60 °C, aqueous NH<sub>4</sub>OH (25 mL, 25-28% w/w) was added dropwise; the black precipitate was formed and heating continued for 2 hours under N<sub>2</sub> atmosphere. The precipitate was magnetically separated and washed thoroughly with water until the supernatant liquor reached neutrality. The obtained material was dried in oven at 100 °C for 12 hours.

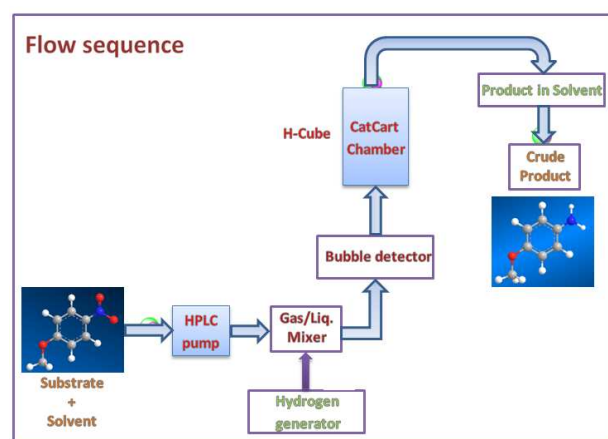


Fig. 1. Schematic representation of flow sequence of reaction.

**Preparation of maghemite-Pd nanocatalyst**

To a stirred mixture of palladium chloride (349 mg) and potassium chloride (1 g) in water (80 mL), maghemite (3 g) was added after 30 minutes. The resulting mixture was stirred at room temperature for 1 hour and the suspension was adjusted to pH 12-13 by slow addition of sodium hydroxide (1.0 M) in 45 minutes and stirring was further continued for 20 hours. The aqueous layer was decanted and ensuing material was washed with distilled water (5 x 50 mL) and dried under vacuum at 60 °C for 12 hours to afford maghemite-Pd nanoparticles. The Pd content was found to be 3.92 % as determined by ICP-MS.

**General procedure for the reduction of nitro compounds**

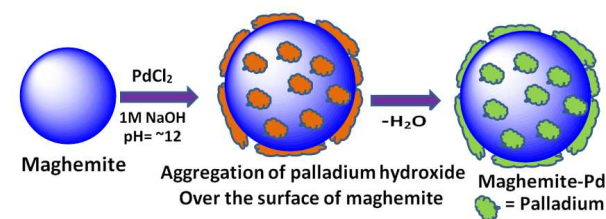
Nitroarene/cyclic nitro compound (1 mmol) was dissolved in 5 mL ethanol:ethyl acetate (1:1) under sonication and reaction mixture was passed through the 30 mm catalyst cartridge, (comprising 160 mg maghemite-Pd (~6.2% Pd content) and 120 mg crushed glass silica) at 30 °C under H<sub>2</sub> pressure (gas flow rate 60 mL/min) with 500 uL min<sup>-1</sup> flow rate. Progress of reaction was monitored by TLC (Thin layer chromatography). The volatiles were evaporated under reduced pressure and, in most cases, the obtained crude material was purified by column chromatography (silica 230–400/alumina; n-hexane: ethyl acetate/MeOH:DCM mixture) and highly polar compound was isolated by crystallization (Table 2, entries 5, 7 and 10).

**General procedure for the reduction of alkenes**

Alkene (1 mmol) was dissolved in 5 mL ethanol under sonication and reaction mixture was passed through the catalyst cartridge (same cartridge as described earlier) at 50 °C under H<sub>2</sub> pressure (gas flow rate 60 mL/min) with 300 uL min<sup>-1</sup> flow rate. The collected volatiles were evaporated under reduced pressure to obtain corresponding products which are further analyzed by GC with corresponding authentic sample to obtain the conversions and yields.

**Results and discussion**

Maghemite-Pd nanocatalyst was prepared by the wet impregnation method followed by dehydration process (Scheme 1).<sup>9b</sup> A transmission electron microscope (TEM) was employed to evaluate size, distribution, and morphology of the synthesized maghemite-Pd nanocomposites. X-ray photoelectron spectroscopy (XPS) characterization was conducted to monitor the surface composition and valence states. Chemical analysis was carried out using the field-emission gun - scanning electron microscopy-electron dispersive spectrometry (FEG-SEM-EDS) and high angle annular dark-field scanning transmission electron microscopy (HAADF-STEM) techniques to identify the various elements.



Scheme 1. Synthesis of maghemite-Pd nanocatalyst.

The XRD patterns of the maghemite and maghemite-Pd nanocomposite are shown in Fig. 2. In both profiles, all the peaks are identified with maghemite ( $\gamma$ -Fe<sub>2</sub>O<sub>3</sub>) structure; the presence of reflections at (110), (210), and (211) supports the occurrence of maghemite with partially ordered vacancies (PDF card 01-089-5892). Further,

Rietveld analysis was performed on both XRD patterns to calculate the lattice parameter of maghemite ( $a = 8.355 \text{ \AA}$ ) and the average crystalline domain size is calculated using broadening of most intense peaks implying the crystallite sizes of the samples in nanometer dimensions ( $\sim 15 \text{ nm}$ ). Palladium related diffraction peaks are barely extractable from XRD pattern of maghemite-Pd nanocomposite which can be attributed either to its low percentage or the very reduced size of the Pd particles ( $< 3 \text{ nm}$ ).<sup>10</sup>

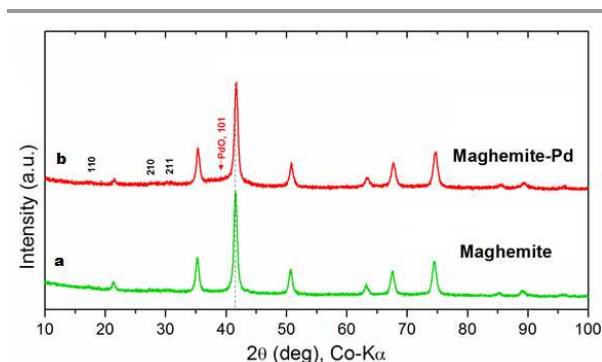


Fig. 2. X-ray diffraction patterns of (a) maghemite and (b) maghemite-Pd. The dotted line indicates the position of the main peak (311) of maghemite for observing the change in diffractogram during the course of reaction.

Fig. 3 shows the TEM image of the maghemite-Pd catalyst with nearly spherical geometry of maghemite support having the size in the range of 10-30 nm, thus corroborating the average size determination of maghemite from XRD. The maghemite nanoparticles are homogeneously covered by Pd nanoparticles – the fact explaining the absence of Pd peaks in the XRD pattern of maghemite-Pd nanocomposite. The measurement of the size of Pd NPs by HRTEM clearly indicates the presence of ultra-small Pd nanoparticles (1-3 nm) (Figure 3c,d). Furthermore, morphology of maghemite-Pd after 12<sup>th</sup> consecutive cycles were verified by TEM, no major visible changes in the morphology was observed (Fig. S1; b, ESI).

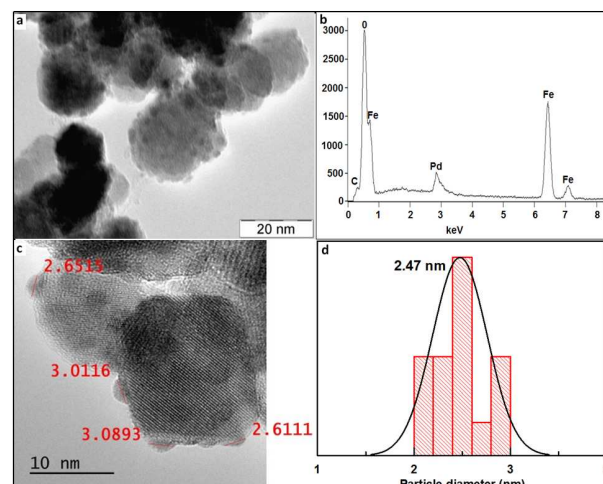


Fig. 3. (a) TEM image of maghemite-Pd nanocomposites showing ultra-small Pd nanoparticles ( $\sim 3 \text{ nm}$ ) covering the surface of maghemite nanoparticles (10-30 nm); (b) SEM-EDS spectrum which indicates the presence of palladium, iron, and oxygen; (c) HRTEM image of maghemite-Pd showing Pd nanoparticles on the surface; (d) Histogram showing Pd nanoparticles in the range of 1-3 nm.

To explore the chemical nature of palladium in maghemite-Pd sample, XPS analysis was performed for the freshly prepared maghemite-Pd and the reused catalyst after 12<sup>th</sup> reactions cycles (Fig. 4); XPS spectra of both samples exhibit dominantly Pd(0) and PdO species without any significant change after recycling (Fig. 4). The most intense peaks of doublet in maghemite-Pd sample at 335.50 eV and 340.76 eV are assignable to metallic Pd(0) and the second weaker set of peaks at 336.81 eV and 342.07 eV could be assigned to Pd(II) in oxidized form such as PdO.<sup>11</sup> Thus, TEM data clearly manifest that maghemite-Pd nanocatalyst is composed of globular maghemite (10-30 nm) nanoparticles. Palladium particles are predominantly in the form of metallic Pd with the minor presence of PdO.

## ARTICLE

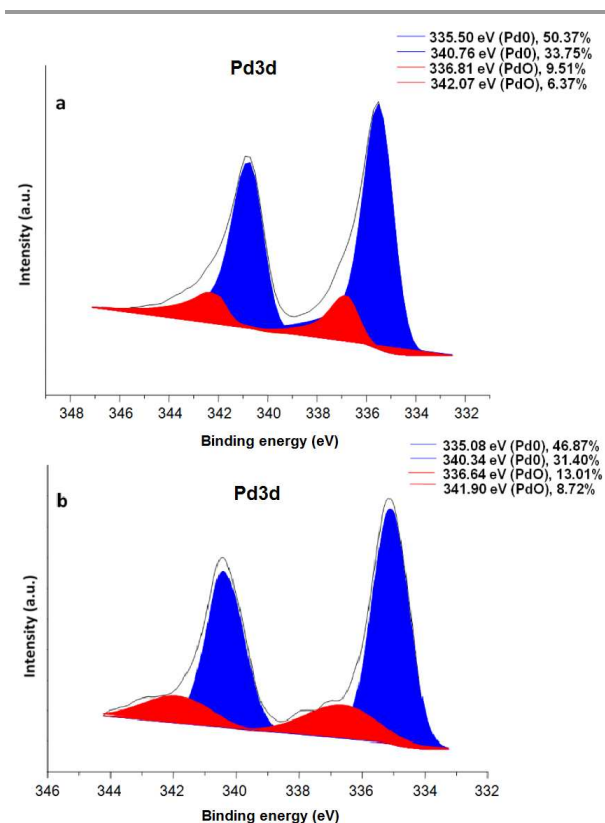


Fig. 4 XPS spectrum of (a) maghemite-Pd nanocatalyst and (b) recycled maghemite-Pd after 12<sup>th</sup> reactions; position of the metallic Pd(0) and PdO are denoted in blue and red colour, respectively.

To distinguish chemical components in the nanocomposite and chemical nature of magnetic support (maghemite vs magnetite), HAADF-STEM and Mössbauer spectroscopy was conducted. High angle annular dark-field scanning transmission electron microscopy (Fig. 5) confirmed that Pd nanoparticles (green) functionalize the iron oxide surface very homogeneously.

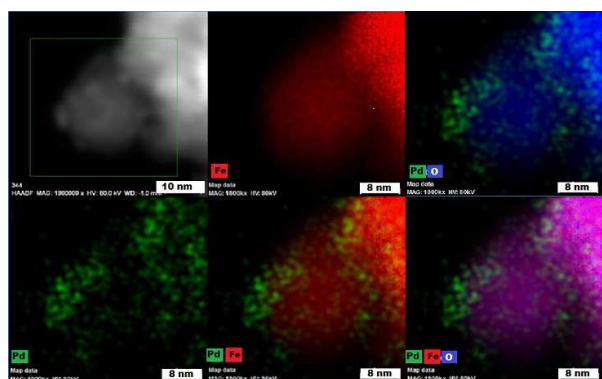


Fig. 5 High angle annular dark-field scanning transmission electron microscopy (HAADF-STEM) images showing elemental mapping of Pd, Fe, and O atoms.

<sup>57</sup>Fe Mössbauer spectroscopy on maghemite-Pd was carried out to clarify the oxidation state of Fe ions in

synthesized and recycled samples as XRD data cannot distinguish between maghemite and magnetite unambiguously. The recorded room temperature/zero-field (300 K/0 T) and low temperature in-field Mössbauer spectra (5 K/5 T) are shown in Fig. 6 and the values of the Mössbauer hyperfine parameters, derived from the spectra fitting, are listed in Table S1, ESI.

The room temperature Mössbauer spectra of synthesized maghemite-Pd and recovered maghemite-Pd samples show one asymmetrical sextet component (Fig. 6a, c). The profiles of the spectra are typical of  $\gamma$ -Fe<sub>2</sub>O<sub>3</sub> phase with iron cations solely in the Fe<sup>3+</sup> oxidation state.<sup>12</sup> The Mössbauer spectra were recorded at low temperature (5 K) to facilitate the resolution of Mössbauer resonant lines via application of an external magnetic field of 5 T. The Mössbauer spectra of both samples are well fitted with two sextets (Fig. 6b, d). The first sextet with a lower isomer shift ( $\delta$ ) and higher hyperfine magnetic field ( $B_{\text{eff}}$ ) corresponds to Fe<sup>3+</sup> ions in the tetrahedral sites (T-sites) of the spinel  $\gamma$ -Fe<sub>2</sub>O<sub>3</sub> crystal structure while the second sextet with a higher  $\delta$  and lower  $B_{\text{eff}}$  is ascribable to Fe<sup>3+</sup> ions occupying the octahedral sites (O-sites) in the  $\gamma$ -Fe<sub>2</sub>O<sub>3</sub> crystal structure.

For the synthesized sample, the spectral ratio between the T-sextet to O-sextet is very close to 0.6 (Fig. 6b) indicating a stoichiometric nature of maghemite with vacancies present only in the O-sites. However, after the reaction, for recovered sample (Fig. 6d), the spectral ratio of T:O is below 0.5 which reflects partially non-stoichiometric character of maghemite particles probably due to occurrence of vacancies at the T sites. In summary, in-field Mössbauer data confirm well stoichiometric maghemite structure with no indications of Fe(II) ions. Similarly, after the sample recycling, there is no remarkable change in the structure/valence state of magnetic support. This fact reflects, together with previously discussed XPS data, the stability of maghemite-Pd nanocatalyst keeping its chemical nature/crystal structure after recycling. As per analysis, we observed that the hyperfine parameters slightly changed which might be due to small changes in the iron surroundings or palladium in the sample after the reaction.

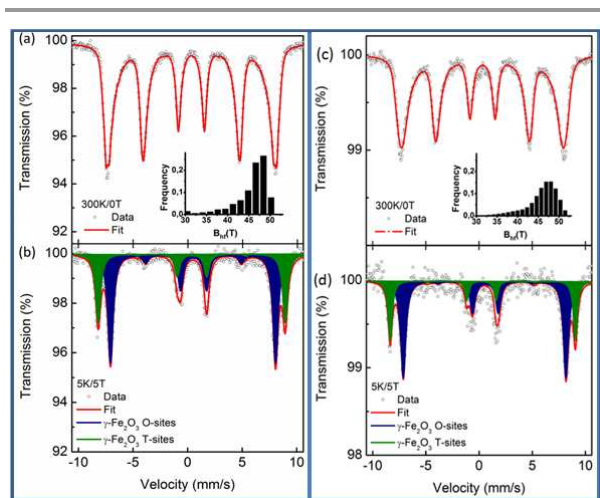


Fig. 6.  $^{57}\text{Fe}$  Mössbauer spectra of the maghemite-Pd sample (left) and recovered sample (after 12 cycles, right), recorded at room temperature and without an external magnetic field (a,c), and at a temperature of 5 K and in external magnetic field of 5 T (b,d). Insets in figures (a,c) show the distribution of the hyperfine magnetic field used for the evaluation of the room temperature spectra.

The applicability of the maghemite-Pd nanocatalyst was evaluated in the reduction of nitroarenes using 4-methoxy nitrobenzene as model substrate in ethanol at 30 °C (Table 1). First, the control reaction was conducted with only maghemite; in the absence of palladium, no product formation was observed (Table 1, entry 1).

Table 1. Optimization of the reaction.<sup>a</sup>

Entry	Catalyst	Temp.	<sup>b</sup> Conversion (%)	Isolated yield (%)
1	Maghemite	70 °C	-	-
2	Maghemite-Pd (9 %)	70 °C	>99	94
3	Maghemite-Pd (7%)	70 °C	>99	95
4	Maghemite-Pd (7%)	30 °C	>99	93
5	Maghemite Pd (6.2%)	30 °C	>99	94
6	Maghemite Pd (6.2%)	30 °C	>81	72 <sup>c</sup>
7	Maghemite Pd (3.9%)	30 °C	>65	53

<sup>a</sup>Reaction conditions: 4-methoxy nitrobenzene (1 mmol), maghemite-Pd (wt%), EtOH (5 mL), Flow rate (500  $\mu\text{L min}^{-1}$ ),  $\text{H}_2$  (gas flow rate 60 mL/min).

<sup>b</sup>Conversion calculated on the basis of GC analysis. <sup>c</sup> $\text{H}_2$  (30 mL/minute).  $t_r$  = 0.75 min.

The optimized reaction conditions were identified by conducting a series of experiments with different catalyst loadings and variation of temperature. The results revealed that full conversion could be achieved with ~6.2 wt % catalyst loading using hydrogen in full mode (full  $\text{H}_2$  mode which corresponds to a gas flow rate 60 mL/min.) with 500  $\mu\text{L min}^{-1}$  flow rate (Table 1, entries 2-5), while 30 mL/min hydrogen pressure showed 81% conversion (Table 1, entry 6). It was noticed that low loading of catalyst (3.92%) showed only 65% conversion (Table 1, entry 7). These optimized reaction conditions were then applied to the reduction of a variety of substrates bearing additional and reducible functional groups (-CONH<sub>2</sub>, -SMe, -CN, -OH, -SO<sub>2</sub>NH<sub>2</sub>, -COOH etc.) attached to the aromatic ring (Table 2).

In all cases, excellent yields of amines (92-98%) were obtained by just passing the solution of nitroarenes in ethanol:ethyl acetate (1:1) through the catalyst cartridge (Table 2, entries 1-8), the only exceptions being 4-nitrobenzonitrile and 4-nitrobenzoic acid which afforded 87% and 88% isolated yields, respectively (Table 2, entries 9, 10). The use of ethyl acetate was found beneficial as it helps improve the solubility of nitroarenes. Among acyclic compounds, nitrocyclopentane gave high yield (93%) of cyclopentyl amine, with no detectable side products, although mechanistically the formation of amine proceeds via the intermediacy of nitroso derivatives and hydroxylamine species;<sup>13</sup> the formation of hydroxylamines during the catalytic hydrogenation is often implicated in the ensuing explosions.<sup>13</sup> Azido functionality is often deployed in organic synthesis and usually serves as a latent amino group which can be revealed in to an amine via reduction. The optimized conditions were utilized for the reduction of 1-azido-4-methylbenzene and 1-azido-4-methoxy benzene which afforded excellent yields of products in 93% and 95%, respectively (Table 2, entries 11 and 12). Similarly, the reduction for N-benzyl-4-nitroaniline gave debenzylated benzene-1-4-diamine with 86% yield (Table 2, entry 13).

The viability of the catalytic system was further explored for the reduction of several of substituted alkenes using  $\text{H}_2$  gas flow rate 60 mL/min (full mode) at 50 °C (Table 3). In this case, ethyl benzene and 3-amino ethyl benzene, 4-methoxy benzene and 1,2-diphenyl ethane were obtained in nearly quantitative conversion, while 4-fluoro ethyl benzene and cyclooctene were obtained in >98% and >91% conversion, respectively. It was observed that by increasing the flow rate from 300 to 500  $\mu\text{L min}^{-1}$ , reaction was incomplete and some unreacted starting material remained. Additionally, methyl cinnamate and methyl 3-(4-methoxyphenyl)acrylate underwent efficient hydrogenation with a flow rate of 300  $\mu\text{L min}^{-1}$  at 70 °C (Table 3, entries 7 and 8).

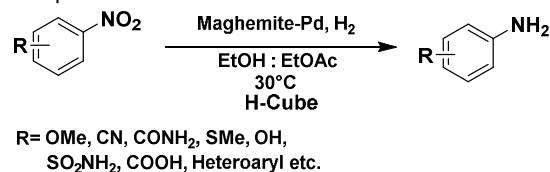
The salient beneficial feature of the reduction under flow conditions has been towards the recyclability of the catalyst. It is important to note that this magnetic support (maghemite) plays a crucial role in the successful reusability

## ARTICLE

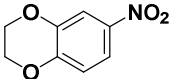
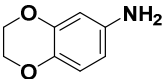
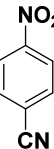
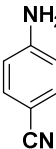
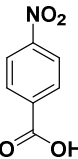
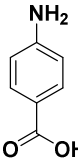
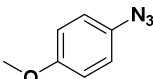
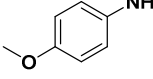
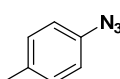
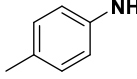
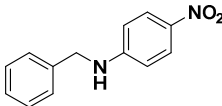
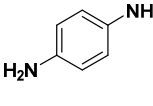
of the catalysts. Due to presence of hydroxyl group on the surface of maghemite support, there is sturdy interaction between maghemite and Pd NPs, which certainly results in minimal leaching of Pd. The developed catalyst was reused and recycled for 12 times successfully with excellent

conversion and yield without any reactivation which are important performance metrics for cost-effective industrial processes (see Table S2, ESI). The ICP-MS analysis indicates 0.000126, 0.000121, 0.000113 Pd% leaching after first, third and seven reaction cycles.

**Table 2.** Reduction of nitro and azide compounds.<sup>a</sup>

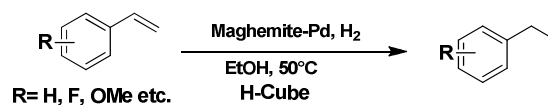


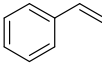
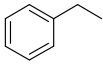
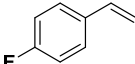
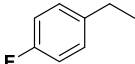
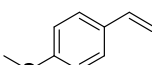
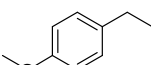
Entry	Substrate	Product	<sup>b</sup> Yield%
1			94
2			94
3			94
4			92
5			98 <sup>c</sup>
6			93 <sup>d</sup>
7			95 <sup>c</sup>

8			95
9			87
10			88 <sup>c</sup>
11			93
12			95
13			86 <sup>e</sup>

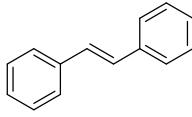
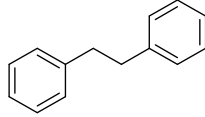
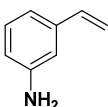
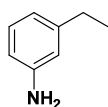
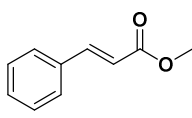
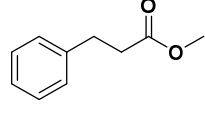
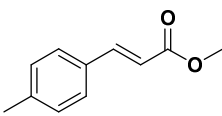
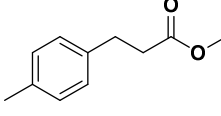
<sup>a</sup>Reaction conditions: nitro compound (1 mmol), maghemite-Pd (6.2 wt %), EtOH:EtOAc (5 mL, 1:1), Temp 30°C, Flow rate (500  $\mu\text{L min}^{-1}$ ),  $\text{H}_2$  (gas flow rate 60 mL/min),  $t_r = 0.75$  min. <sup>b</sup>Isolated yield. <sup>c</sup>Isolated by crystallization. <sup>d</sup>Isolated as hydrochloride salt. <sup>e</sup>N-benzyl-4-nitroaniline (0.5 mmol), maghemite-Pd (6.2 wt %), EtOAc:EtOH (12 mL, 5 : 1), Temp 70°C, 300  $\mu\text{L min}^{-1}$ ,  $t_r = 1.25$  min.

Table 3. Reduction of alkenes.<sup>a</sup>



Entry	Substrate	Product	<sup>b</sup> Conversion (%)	<sup>c</sup> Yield %
1			>99	95 <sup>d</sup>
2			>98	93 <sup>d</sup>
3			>99	96 <sup>d</sup>
4			>91	86 <sup>d</sup>

## ARTICLE

				
5			>99	94 <sup>d</sup>
6			>99	93 <sup>d</sup>
7			>99	94 <sup>e</sup>
8			>99	95 <sup>e</sup>

<sup>a</sup>Reaction conditions: Substrate (1 mmol), maghemite-Pd (6.2 wt %), EtOH (5mL), Temp. 50°C, Flow rate 300  $\mu\text{L min}^{-1}$ ,  $\text{H}_2$  (gas flow rate 60 mL/min),  $t_r = 0.75$  min. <sup>b</sup>Conversions calculated on the basis of GC analysis, <sup>c</sup>isolated yield, <sup>d</sup>Yields are determined by GC against internal integration. <sup>e</sup>Temp. 70 °C, Isolated yields.

The hydrogenation reactions, catalyzed by maghemite-Pd nanocomposites, in continuous flow mode have several advantages relative to batch processes, where unique solid-gas-liquid triphasic reaction conditions prevail during the hydrogenation reactions.<sup>14</sup> Most of the reported traditional catalysts are deployed under homogeneous conditions and are not reusable, making the protocol expensive.<sup>15</sup> Also, the present catalytic protocol is comparable with reported methods used in continuous flow methods (Table S3 and S4). In contrast, maghemite-Pd nanocomposites, could be easily retrievable and reused for several reaction cycles with barely observable leaching of Pd metal, which renders this catalytic protocol truly sustainable. Additionally, no hydrogen balloon/gas cylinder is used for the reactions, as in-situ generated hydrogen gas from water certainly increases the safety aspects.<sup>16</sup> We believe that several other hydrogenation reactions could be performed using this catalyst.

## Conclusions

In summary, we have developed continuous flow hydrogenation protocols for the reduction of nitroarenes, azides, and alkenes catalyzed by ultra-fine (1-3 nm) Pd nanoparticles supported on recyclable maghemite support. The corresponding products were obtained in good to excellent yield under continuous flow and without any requirements for filtration. The stability of nanocatalyst was found to be impeccable with the added advantage that it could be used employed successively 12 times without

major loss of its activity. The structure and morphology of reused catalyst was confirmed by X-ray photoelectron spectroscopy and transmission electron microscopy analysis. Notably, a very negligible leaching of Pd metal was observed and Pd species remained intact throughout the reaction cycles. The catalyst described in this work provides clear advantages in terms of environmental impact due to lower metal loading, and no requirements of other additives which bodes well for its adoption in industrial process. The results obtained are of importance to improvement of sustainable protocols for fine-chemicals and, particularly for the large scale reactions.

## Acknowledgements

The authors thank Jana Straska for TEM and Martin Kuba for ICP-MS analysis. The authors acknowledge support from the Ministry of Education, Youth and Sports of the Czech Republic (LO1305) and by the Operational Program Education for Competitiveness - European Social Fund (project CZ.1.07/2.3.00/30.0041 and CZ.1.07/2.4.00/31.0189) of the Ministry of Education, Youth and Sports of the Czech Republic. The work is also funded by the Palacky University Institutional support and IGA grant (Project No. IGA-PrF-2015-017).

## References

- 1 M. Baghbanzadeh, T. N. Glasnov, and C. O. Kappe, *J. Flow Chem.*, 2013, **3**, 109-113.
- 2 (a) Y. Jang, S. Kim, S. W. Jun, B. H. Kim, S. Hwang, I. K. Song, B. M. Kim, and T. Hyeon, *Chem. Commun.*, 2011, **47**, 3601-3603; (b) V. Pandarus, R. Ciriminna, F. B eland, and M. Pagliaro, *Adv. Synth. Catal.*, 2011, **353**, 1306-1316; (c) J. Li, X.-Y. Shi, Y.-Y. Bi, J.-F. Wei, and Z.-G. Chen, *ACS Catal.* 2011, **1**, 657-664; (d) F.-X. Felpin and E. Fouquet, *Chem. Eur. J.*, 2010, **16**, 12440-12445.
- 3 (a) G. Liang, H. Cheng, W. Li, L. He, Y. Yu, and F. Zhao, *Green Chem.* 2012, **14**, 2146-2149; (b) U. Sharma, P. Kumar, N. Kumar, V. Kumar, and B. Singh, *Adv. Synth. Catal.*, 2010, **352**, 1834-1840; (c) M. B. Gawande, H. Guo, A. K. Rath, P. S. Branco, Y. Chen, R. S. Varma, and D.-L. Peng, *Rsc Adv.*, 2013, **3**, 1050-1054; (d) M. B. Gawande, A. K. Rath, P. S. Branco, I. D. Nogueira, A. Velhinho, J. J. Shrikhande, U. U. Indulkar, R. V. Jayaram, C. A. A. Ghumman, N. Bundaleski, and O. M. N. D. Teodoro, *Chem. Eur. J.*, 2012, **18**, 12628-12632.
- 4 (a) T. Marimuthu, and H. B. Friedrich, *ChemCatChem* 2012, **4**, 2090-2095; (b) Y. Monguchi, Y. Fujita, S. Hashimoto, M. Ina, T. Takahashi, R. Ito, K. Nozaki, T. Maegawa, and H. Sajiki, *Tetrahedron* 2011, **67**, 8628-8634; (c) O. Verho, A. Nagendiran, E. V. Johnston, C.-W. Tai, and J.-E. Baeckvall, *ChemCatChem* 2013, **5**, 612-618; (d) Z. Sun, H. Zhang, G. An, G. Yang, and Z. Liu, *J. Mater. Chem.*, 2010, **20**, 1947-1952; (e) M. K. Basu, F. F. Becker, and B. K. Banik, *Tetrahedron Lett.*, 2000, **41**, 5603-5606; (f) A. Stolle, T. Szuppa, S. E. S. Leonhardt, and B. Ondruschka, *Chem. Soc. Rev.*, 2011, **40**, 2317-2329; (g) C.-H. Pelisson, A. Denicourt-Nowicki, C. Meriadec, J.-M. Greneche, and A. Roucoux, *ChemCatChem* 2015, **7**, 309-315.
- 5 (a) F. Mastronardi, B. Gutmann, and C. O. Kappe, *Org. Lett.*, 2013, **15**, 5590-5593; (b) M. Damm, B. Gutmann, and C. O. Kappe, *ChemSusChem* 2013, **6**, 978-982; (c) D. Obermayer, A. M. Balu, A. A. Romero, W. Goessler, R. Luque, and C. O. Kappe, *Green Chem.*, 2013, **15**, 1530-1537; (d) K. R. Knudsen, J. Holden, S. V. Ley, and M. Ladlow, *Adv. Synth. Catal.*, 2007, **349**, 535-538; (e) M. M. Moghaddam, B. Pieber, T. Glasnov, and C. O. Kappe, *ChemSusChem* 2014, **7**, 3122-3131; (f) T. Ouchi, C. Battilocchio, J. M. Hawkins, and S. V. Ley, *Org. Process Res. Dev.*, 2014, **18**, 1560-1566; (g) M. V. Rojo, L. Guetzoian, and I. R. Baxendale, *Org. Biomol. Chem.*, 2015, **13**, 1768-1777; (h) E. Alza, C. Rodriguez-Esrich, S. Sayalero, A. Bastero, and M. A. Pericas, *Chem. Eur. J.*, 2009, **15**, 10167-10172; (i) C. Ayats, A. H. Henseler, E. Dibello, and M. A. Pericas, *ACS Catal.*, 2014, **4**, 3027-3033; (j) S. L. Bourne, P. Koos, M. O'Brien, B. Martin, B. Schenkel, I. R. Baxendale, S. V. Ley, *Synlett* 2011, 2643-2647; (k) J. Izquierdo, C. Ayats, A. H. Henseler, and M. A. Pericas, *Org. Biomol. Chem.*, 2015, **13**, 4204-4209; (l) C. B. Kelly, C. Lee, and N. E. Leadbeater, *Tetrahedron Lett.*, 2011, **52**, 263-265; (m) R. Martin-Rapun, S. Sayalero, and M. A. Pericas, *Green Chem.*, 2013, **15**, 3295-3301.
- 6 (a) A. Kawanishi, C. Miyamoto, Y. Yabe, M. Inai, T. Asakawa, Y. Hamashima, H. Sajiki, and T. Kan, *Organic Lett.*, 2013, **15**, 1306-1309; (b) M. Cano, A. M. Benito, W. K. Maser, and E. P. Urriolabeitia, *New J. Chem.*, 2013, **37**, 1968-1972.
- 7 (a) J. D. Lewis, S. Van de Vyver, A. J. Crisci, W. R. Gunther, V. K. Michaelis, R. G. Griffin, and Y. Rom an-Leshkov, *ChemSusChem* 2014, **7**, 2255-2265; (b) P. N. Liu, P. M. Gu, F. Wang, and Y. Q. Tu, *Org. Lett.*, 2004, **6**, 169-172; (c) M. Irfan, T. N. Glasnov, C. O. Kappe, *ChemSusChem* 2011, **4**, 300-316.
- 8 D. Cantillo, and C. O. Kappe, *ChemCatChem* 2014, **6**, 3286-3305.
- 9 (a) M. B. Gawande, P. S. Branco, and R. S. Varma, *Chem. Soc. Rev.*, 2013, **42**, 3371-3393; (b) M. B. Gawande, R. Luque, and R. Zboril, *ChemCatChem* 2014, **6**, 3312-3313; (c) M. B. Gawande, A. K. Rath, J. Tucek, K. Safarova, N. Bundaleski, O. M. N. D. Teodoro, L. Kvitek, R. S. Varma, and R. Zboril, *Green Chem.*, 2014, **16**, 4137-4143; (d) D. Wang, D. Astruc, *Chem. Rev.*, 2014, **114**, 6949-6985; (e) R. B. Nasir Baig, and R. S. Varma, *Green Chem.*, 2013, **15**, 398-417; (f) M. B. Gawande, Y. Monga, R. Zboril, and R. K. Sharma, *Coord. Chem. Rev.*, 2015, **288**, 118-143; (g) S. D. Shelke, S. R. Bankar, G. R. Mhaske, S. S. Kadam, D. K. Murade, S. B. Bhorkade, A. K. Rath, N. Bundaleski, O. M. N. D. Teodoro, R. Zboril, R. S. Varma and M. B. Gawande, *ACS Sustainable Chem. Eng.*, 2014, **2**, 1699-1706.
- 10 S. Akbayrak, M. Kaya, M. Volkan, and S.  zkar, *Appl. Catal. B.*, 2014, **147**, 387-393.
- 11 M. Liao, Q. Hu, J. Zheng, Y. Li, H. Zhou, C.-J. Zhong, and B. H. Chen, *Electrochim. Acta* 2013, **111**, 504-509.
- 12 (a) R. Zboril, M. Mashlan, and D. Petridis, *Chem. Mater.*, 2002, **14**, 969-982; (b) J. Tucek, R. Zboril, and D. Petridis, *J. Nanosci. Nanotechnol.*, 2006, **6**, 926-947.
- 13 D. Cantillo, M. M. Moghaddam, and C. O. Kappe, *J. Org. Chem.*, 2013, **78**, 4530-4542.
- 14 M. Irfan, T. N. Glasnov, and C. O. Kappe, *ChemSusChem* 2011, **4**, 300-316.
- 15 M. A. Mercadante, C. B. Kelly, C. Lee, and N. E. Leadbeater, *Org. Process Res. Dev.*, 2012, **16**, 1064-1068.
- 16 R. V. Jones, L. Godorhazy, N. Varga, D. Szalay, L. Urge, and F. Darvas, *J. Comb. Chem.* 2006, **8**, 110-116.

## Table of Content

